*Pure Appl. Chem.*, Vol. 74, No. 9, pp. 1773–1783, 2002.


# Functional nanoparticle architectures for sensoric, optoelectronic, and bioelectronic applications*

Itamar Willner‡ and Bilha Willner

*Institute of Chemistry, Farkas Center for Light-Induced Processes, Hebrew University of Jerusalem, Jerusalem 91904, Israel*

*Abstract*: Tailored sensoric, electronic, photoelectrochemical, and bioelectrocatalytic functions can be designed by organized molecular or biomolecular nanoparticle hybrid configurations on surfaces. Layered receptor-cross-linked Au nanoparticle assemblies on electrodes act as specific sensors of tunable sensitivities. Layered DNA-cross-linked CdS nanoparticles on electrode supports reveal organized assemblies of controlled electronic and photoelectrochemical properties. Au nanoparticle-FAD semisynthetic cofactor units are reconstituted into apo-glucose oxidase (GOx) and assembled onto electrodes. The resulting enzymes reveal effective electrical contacting with the electrodes, and exhibit bioelectrocatalytic functions toward the oxidation of glucose to gluconic acid. Magneto-switchable electrocatalysis and bioelectrocatalysis are accomplished by the surface modification of magnetic particles with redox-relay units. By the attraction of the modified magnetic particles to the electrode support, or their retraction from the electrode, by means of an external magnet, the electrochemical functions of the magnetic particle-tethered relays can be switched between "ON" and "OFF" states, respectively. The magneto-switchable redox functionalities of the modified particles activate electrocatalytic transformations, such as a biocatalytic chemoluminescence cascade that leads to magneto-switchable light emission or the activation of bioelectrocatalytic processes.

Capping of nanoparticles with molecular monolayers or thin films may introduce functional units such as recognition sites, catalytic elements, redox-active groups or bioactive components [1]. The surface modifier of the particles may then be used to couple the unique electronic, photonic, or catalytic properties of quantum-size nanoparticles with molecular or macromolecular functionalities to yield hybrid systems of new features [2]. For example, nucleic acid-functionalized Au nanoparticles, exhibiting a characteristic red color originating from the single-particle plasmon exciton, that are complementary to the two ends of a target DNA, turn blue upon hybridization with the target DNA due to the formation of an interparticle-coupled plasmon exciton [3]. Quantization of the double-layer capacitance charging of alkanethiol-functionalized Au nanoparticles is a property of the monolayer capping and nanoparticle core hybrid system. The capacitance generated by the ionic space charge upon the charging of the metal core was found to be controlled by the thickness of the dielectric medium of the monolayer, and the charging of nanocapacitors by single electrons occurs at quantized potential intervals ($\Delta V = e/C$), determined by the nanoparticle hybrid composition [4].

*Pure Appl. Chem.* **74**, 1489–1783 (2002). An issue of reviews and research papers based on lectures presented at the 2nd IUPAC Workshop on Advanced Materials (WAM II), Bangalore, India, 13–16 February 2002, on the theme of nanostructured advanced materials.
‡Corresponding author

Alternatively, the functionalization of nanoparticles may allow the assembly of surface-confined architectures or patterns [5]. The present account outlines recent advances, originating from our laboratory, that demonstrate the surface modification of metallic, semiconductor, and magnetic particles with functional molecular or biomolecular units, and the use of these hybrid structures as key elements to construct novel sensoric, electronic, optoelectronic, and bioelectronic systems.

## RECEPTOR-CROSS-LINKED Au NANOPARTICLES ON ELECTRODES FOR SENSORIC APPLICATIONS

A layer-by-layer assembly process of citrate-capped Au nanoparticles (12 ± 1 nm) on indium tin oxide (ITO) glass surfaces was developed [6], Scheme 1. First, a transparent ITO conductive glass support is functionalized with a 3-aminopropylsiloxane thin film. Electrostatic binding of the negatively charged citrate-capped Au nanoparticles, followed by the electrostatic association of the oligocationic *bis*-paraquat-*p*-phenylene (**1**), yields the first nanoparticle layer. By a subsequent stepwise treatment of the surface with the Au nanoparticles and (**1**), a controlled number of Au nanoparticles associated with the surface are constructed. Figure 1A shows the absorption spectra of the system upon the build-up of the

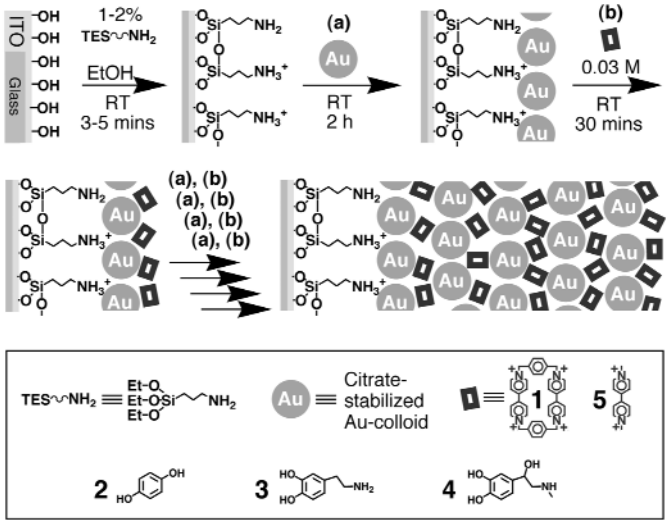


**Scheme 1** Assembly of a layered receptor-cross-linked Au nanoparticle array for the electrochemical sensing of π-donor substrates.

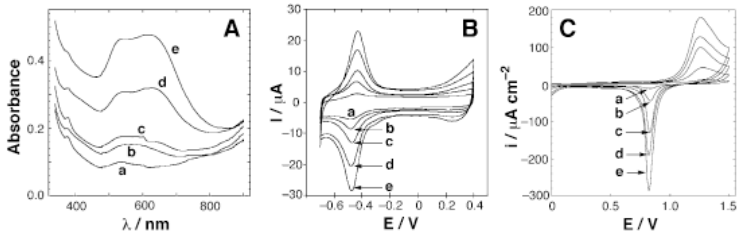


**Fig. 1** Characterization of the (**1**)-cross-linked Au nanoparticle array upon the build-up of one to five layers (a) to (e): (A) the absorption spectra of the arrays; (B) cyclic voltammograms of the (**1**)-cross-linking units, recorded in 0.1 M phosphate buffer, pH = 7.2, under Ar, scan rate 100 $mV \cdot s^{-1}$; (C) cyclic voltammograms corresponding to the Au nanoparticles, recorded in 1.0 M $H_2SO_4$, under Ar, scan rate 50 $mV \cdot s^{-1}$.

nanoparticle layers. In addition to the increase in the band at $\lambda = 520$ nm, characteristic of the plasmon absorbance of the Au nanoparticles, a new absorbance, $\lambda = 650$ nm is observed. The latter absorbance band is attributed to an interparticle-coupled plasmon exciton that originates from the clustering of the particles on the surface. As the number of aggregated particles is higher, the probability for such coupled plasmon excitations increases. Figure 1B shows the cyclic voltammograms of the *bis*-(paraquat)-*p*-phenylene oligocationic cross-linker (**1**) units, observed upon the construction of the layered assembly. The electrical response of (**1**) increases almost linearly upon the build-up of the assembly, implying a three-dimensional conductivity of the array. By coulometric assay of the reduction wave of (**1**), the average surface coverage of (**1**) per layer is estimated to be $1.5 \times 10^{-11}$ mole·cm$^{-2}$. Figure 1C shows the electrical response of the Au nanoparticles (in 1.0 M $H_2SO_4$). These redox waves correspond to the reduction of the Au oxide layer and the surface reoxidation, respectively. The redox response of the Au nanoparticles increases linearly with the number of particle layers, and by coulometric assay of the reduction waves, we estimate that the average surface coverage of the nanoparticles per layer corresponds to $0.8 \times 10^{11}$ particles·cm$^{-2}$. Knowing the surface coverage per layer of (**1**), we find that ca. 100 oligocationic cross-linking units of (**1**) are associated with each particle.

The molecular oligocationic cross-linker (**1**) exhibits π-acceptor properties, and π-donor substrates of appropriate size can bind to the cavity of (**1**). The resulting supramolecular complex is stabilized by π-donor–acceptor interactions. Formation of such supramolecular complexes on the nanoengineered three-dimensional array of nanoparticles would concentrate the π-donor substrate at the electrode surface, and enhanced sensitivity would be accomplished. Also, the sensitivity of the functional electrodes would be controlled by the number of nanoparticle layers associated with the conductive support. Furthermore, the three-dimensional conductivity of the array suggests that the π-donor encapsulated in the π-acceptor receptor units could be sensed electrochemically, provided that the π-donor compound is redox-active. Indeed, a series of π-donor substrates such as hydroquinone (**2**), dopamine (**3**), and adrenaline (**4**) was electrochemically sensed by such functional electrodes [6]. Figure 2 shows the cyclic voltammograms of the functional electrode consisting of 5 layers of (**1**)-cross-linked Au nanoparticles upon the analysis of different concentrations of adrenaline (**4**). The electrical response of (**4**) increases as the bulk concentration is elevated, and Figure 2 (inset) depicts the derived calibration curve. It should be noted that an analogous 5-layer array of Au nanoparticles cross-linked by *N*,*N*′-dimethyl-4,4′-bipyridinium dichloride (**5**), that was assembled on an ITO electrode, is insensitive toward the electrochemical detection of (**4**) in this concentration range. The dicationic cross-linker (**5**), exhibits substantially lower affinity to form a π-donor–acceptor complex with (**4**). Thus, this control experiment reveals that the successful electrochemical sensing of (**4**) by the nanoparticle-modified electrode, does not originate from the increase in the electrode surface area due to the formation of a rough-

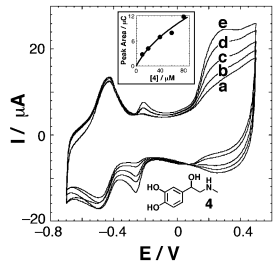


**Fig. 2** Cyclic voltammograms corresponding to the analysis of adrenaline (**4**) by a 5-layer (**1**)-cross-linked array of Au nanoparticles. Concentration of (**4**) corresponds to: (a) $1 \times 10^{-5}$ M; (b) $2 \times 10^{-5}$ M; (c) $4 \times 10^{-5}$ M; (d) $6 \times 10^{-5}$ M; (e) $8 \times 10^{-5}$ M. Data recorded under Ar in 0.1 M phosphate buffer, pH = 7.2, scan rate 100 mV·s$^{-1}$. Inset: Calibration curve corresponding to the amperometric response of the array (at E° = –0.26 V vs. SCE) at variable concentrations of (**4**).

ened surface, but rather from the specific concentration of (**4**) in the π-acceptor receptor sites associated with the functional electrode.

## ELECTRICAL CONTACTING OF ENZYMES BY SINGLE Au NANOPARTICLE ARCHITECTURES

Redox-enzymes lack electron-transfer communication with electrodes. The barrier for electrical contacting of the enzymes with the electrodes may be explained by the Marcus equation, eq. 1, that defines the parameters controlling the electron-transfer rate between a donor–acceptor pair ($\Delta G°$ and $\lambda$ are the free-energy change and reorganization energy accompanying the electron-transfer process, $d$ and $d_o$ correspond to the actual distance separating the donor–acceptor pair and the van der Waals distance between the donor and acceptor, respectively, and $\beta$ is the electron coupling constant).

$$k_{et} \propto \exp[-\beta(d - d_o)] \cdot \exp[(\Delta G° + \lambda)^2 / 4RT\lambda] \quad (1)$$

One may consider the redox-site in proteins and the electrode as a donor–acceptor pair. As the average size of proteins is ca. 40–120 Å, the redox site is embedded in a matrix that spatially separates the donor and acceptor components, leading to the lack of electron-transfer communication between the components. Electrical contacting of redox-enzymes with electrodes was achieved by tethering redox-relays to the proteins, or the immobilization of the enzymes in redox-polymers. Although in these systems the bioelectrocatalytic functions of the enzymes are activated, the electron-transfer turnover rates between the enzymes and the electrode are far slower than the electron-transfer turnover rates with their native enzymes. We have reported that the alignment of redox proteins on surfaces by the surface reconstitution of an apo-flavoenzyme on an electron-relay/flavin adenine dinucleotide (FAD) monolayer, leads to an electrically contacted bioelectrocatalyst with an efficient electron-transfer turnover [7].

Recently, we found that a single Au nanoparticle that is nanoengineered into the protein acts as a nanoelectrode for the contacting of the redox site with macroscopic electrodes [8]. A Au nanoparticle (1.3 ± 0.2 nm) functionalized with a single *N*-succinimidyl active ester group is reacted with $N^6$-(2-aminoethyl)-flavin adenine dinucleotide, $NH_2$-FAD (**6**), Scheme 2. Apo-glucose oxidase, apo-GOx, is then reconstituted with the cofactor-functionalized Au nanoparticles, and the resulting modified protein is linked to a bulk Au electrode functionalized with *bis-p*-xylenedithiol. Microgravimetric quartz-crystal microbalance measurements indicate that the surface coverage of the enzyme is ca. $1 \times 10^{-12}$ mole·cm$^{-2}$. Figure 3 shows the cyclic voltammograms of nanoparticle-functionalized enzyme electrodes at different concentrations of glucose. The resulting bioelectrocatalytic anodic current indi-

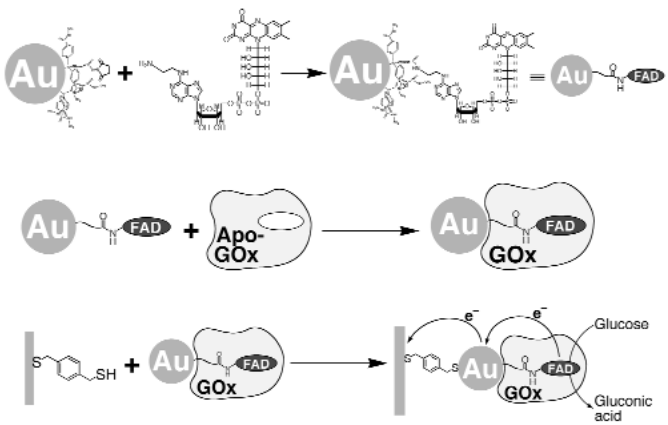


**Scheme 2** Reconstitution of apo-GOx with an FAD-functionalized Au nanoparticle and the assembly of the reconstituted enzyme as a monolayer on an Au electrode.

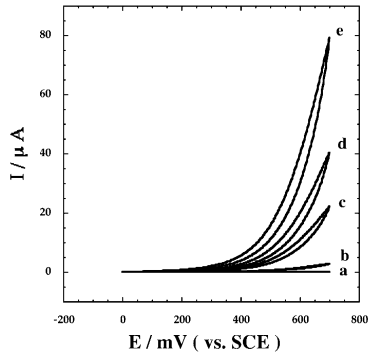


**Fig. 3** Cyclic voltammograms of the FAD-Au nanoparticle-reconstituted GOx electrode in the presence of variable concentrations of glucose corresponding to: (a) 0 M; (b) $1 \times 10^{-3}$ M; (c) $1 \times 10^{-2}$ M; (d) $2 \times 10^{-2}$ M; (e) $5 \times 10^{-2}$ M. Data recorded under Ar, 0.1 M phosphate buffer, pH = 7.0, scan rate 5 mV·s$^{-1}$.

cates that the redox enzyme is electrically contacted with the electrode support. Control experiments reveal that a Au electrode modified with an FAD monolayer on which apo-glucose oxidase is reconstituted, yields an enzyme-electrode that lacks electrical communication with the electrode. Thus, the single Au nanoparticle attached to the FAD site of the enzyme acts as a nanoelectrode for the electrical contacting of the redox enzyme with the bulk electrode. A calibration plot that corresponds to the amperometric responses of the functional electrode at different glucose concentrations was derived. Knowing the surface coverage of the enzyme, and the maximum output current of the system, the electron-transfer turnover rate is estimated to be 2300 $s^{-1}$. This unprecedented efficient electron-transfer communication between the redox protein and the electrode originates from the mediated electron transfer by a single Au nanoparticle that is conjugated to the protein assembly. This effective electron-transfer communication between the nanoengineered redox enzyme and the electrode has important consequences on the sensitivity and selectivity of the enzyme electrode. Glucose concentrations as low as 30 μM are sensed by the system, and the enzyme-electrode is not affected by common glucose-sensing interferants such as ascorbic acid, uric acid, or oxygen.

## NANOPARTICLE-FUNCTIONALIZED DNA STRUCTURES ON SURFACES

Research in the area of nanoparticle-coupled DNA electronics attracts scientific efforts in two general directions: (i) The unique electronic and optical properties of nanoparticles may be used to generate labels of controllable properties. Indeed, metal nanoparticles or nanorods modified with nucleic acids, were used as functional labels for the sensing of DNA [9]. (ii) DNA may be used as a template for the generation of metallic or semiconductive nanostructures [10]. The possibility of synthesizing DNA of predesigned length and shape, the ability to "cut and paste" nucleic acids with appropriate biocatalysts, and the versatile chemical means to functionalize nucleic acids turn DNA into an attractive mold for the deposition of nanostructures [9]. Indeed, a primary study has demonstrated the generation of Ag or Pd wires on DNA templates [10].

We have used nucleic acid-functionalized CdS nanoparticles (2.6 ± 0.4 nm) to construct aggregated arrays of DNA [11], Scheme 3. The CdS particles were functionalized with the thiolated nucleic acids (**7**) and (**8**) that are complementary to the DNA (**9**) (ca. 20–24 nucleic acid residues are associated with each CdS nanoparticle). Scheme 3A shows the assembly of the layered aggregated CdS array on a glass support. Covalent coupling of (**7**) to the maleimide-functionalized siloxane film associated with the glass support yields the active interface for the assembly of the CdS nanoparticle structure. Hybridization of (**9**) with the surface is followed by the hybridization of the (**8**)-functionalized CdS nanoparticles to the single-stranded end of (**9**). The subsequent reaction of the first layer of CdS parti-

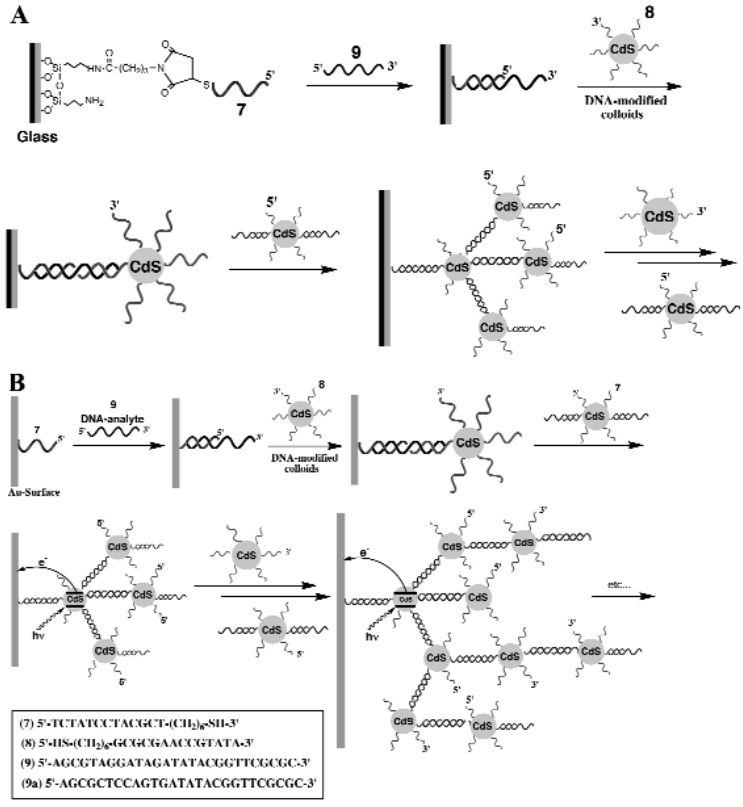


**Scheme 3** Assembly of layered DNA-cross-linked CdS nanoparticle arrays on: (A) a glass support; (B) a Au electrode.

cles with the (**7**)-functionalized CdS particles, pretreated with (**9**), generates the second-layer CdS nanoparticle aggregate. By the stepwise reaction of the interface with either (**7**)-functionalized CdS particles or (**8**)-modified CdS particles that are pretreated with (**9**), a controlled number of aggregated CdS nanoparticles is generated on the surface. In a similar way, an aggregated array of CdS nanoparticle layers is organized on an Au electrode using the thiolated nucleic acid monolayer of (**7**) as the base interface to construct the assembly, Scheme 3B. Figures 4A and 4B show the absorbance and fluorescence spectra of the CdS nanoparticle arrays on the glass surfaces upon the build-up of the aggregated layers, respectively. The large Stokes shift of the fluorescence band suggests that it originates from a surface-trapped electrons. Figure 4C shows the photocurrent action spectra of the CdS nanoparticle array upon the construction of the layered system. The photocurrents increase as the number of CdS particles is elevated, and the photocurrent action spectrum overlaps the absorbance spectrum of the particles (see inset, Fig. 4C), implying that the photocurrent originates from the excitation of the semiconductor nanoparticles. An important question that has to be addressed relates to the mechanism of the electron injection into the electrode support. Whether double-stranded DNA acts as an electron-conducting matrix is still an important scientific enigma. The resulting photocurrent in the CdS nanoparticle array could originate from the direct contact of CdS nanoparticles with the electrode, or from a DNA-assisted tunneling path. We know, however, that the association of $Ru(NH_3)_6^{3+}$ units to the DNA [11] or the intercalation of the electron acceptor, doxorubicin, into the double-stranded DNA, enhances substantially the generated photocurrent in the CdS nanoparticle system [12]. This suggests that electron hopping through the relay units associated with DNA facilitates the transport of electrons from the semiconductor nanoparticles to the electrode.

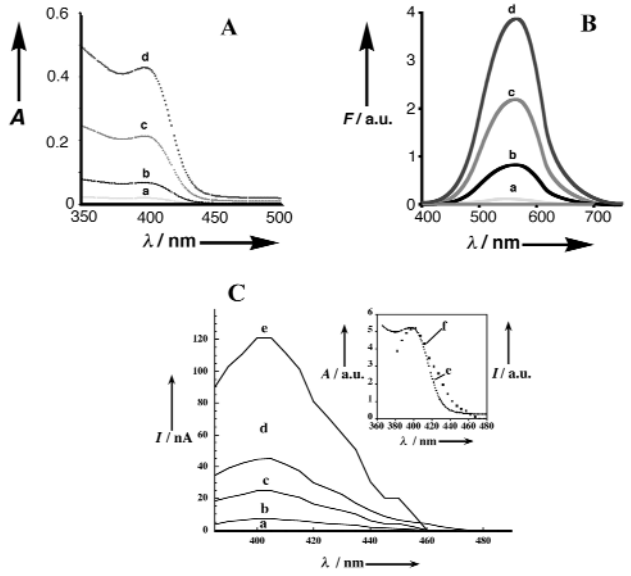


**Fig. 4** Photophysical properties and photoelectrochemical functions of DNA-cross-linked CdS nanoparticle arrays: (A) absorption spectra of 1–4 CdS nanoparticle layers, (a) to (d); (B) fluorescence spectra of 1–4 CdS nanoparticle layers of CdS nanoparticles, $\lambda_{ex} = 405$ nm; (C) photocurrent action spectra of 1–5 layers, (a) to (e), of DNA-cross-linked CdS nanoparticles. Inset: Comparison of the photocurrent spectrum (curve e) and absorption spectrum (curve f) corresponding to a 5-layer DNA-cross-linked CdS array.

The future architecture of complex nanoparticle circuitry will require the nanoengineering of semiconductor or metallic nanoparticles that are linked together by conductive (or semiconductive) nanowires. Toward this goal, we developed a method to generate a Au nanoparticle wire based on DNA [13]. The method is depicted in Scheme 4, where a Au nanoparticle ($1.3 \pm 0.2$ nm) functionalized with the single psoralen (**10**), is intercalated into a polyT/polyA double-stranded DNA. The resulting matrix

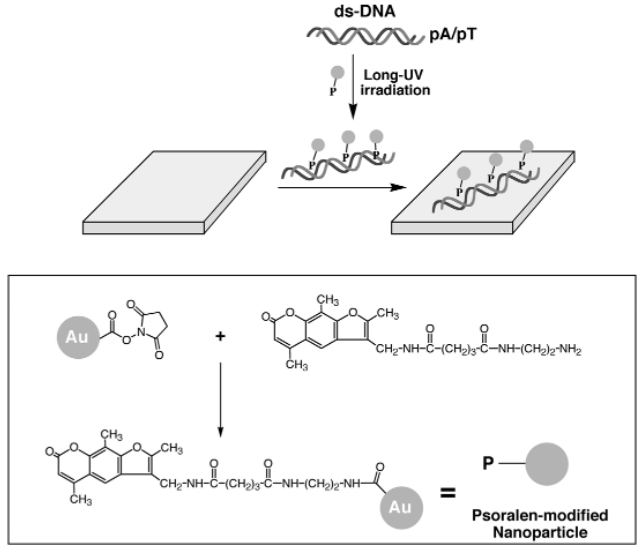


**Scheme 4** Assembly of a Au nanoparticle wire in a pA·pT double-stranded DNA template.

is irradiated to covalently link the psoralen units to the DNA thymine bases [14], and then deposited onto mica. Figure 5 shows the AFM micrograph of the resulting Au nanoparticle wire formed on the DNA template. The wire has a length of 500–600 nm and a width of ca. 3.5 to 8 nm. Although the AFM image of the Au nanoparticle wire indicates a dense particle-contacted assembly, this picture might be misleading due to the size of the scanning tip. Studies to examine the conductivity of the resulting nanoparticle wire are under way in our laboratory, with the possibility of improving the conductivity by the electroless catalytic enlargement of the nanoparticles (cf. Scheme 4).

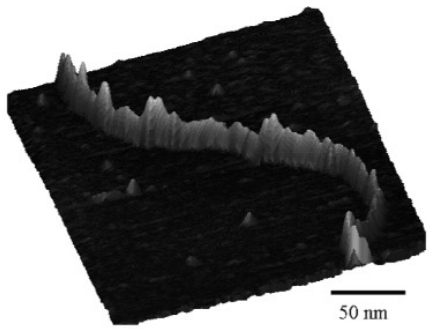


**Fig. 5** AFM image of a Au nanoparticle wire generated on a DNA template.

## FUNCTIONAL MAGNETIC PARTICLES FOR ELECTRONIC AND OPTOELECTRONIC SWITCHING

Functionalized magnetic particles represent hybrid systems where the magnetic particles act as carriers for the chemical functionality associated with them. We have recently applied functional magnetic particles as triggers for the switching of electrocatalytic and bioelectrocatalytic transformations [15]. We exemplify here the magneto-switchable activation and deactivation of the enzyme glucose oxidase, and the magneto-switchable light emission from a system consisting of functionalized magnetic particles, Scheme 5. Magnetite particles (1 μm average diameter) were modified with a [3-(2-aminoethyl)aminopropyl]siloxane film, and *N*-ferrocenylmethyl aminohexanoic acid was covalently linked to the particles to yield the ferrocene-functionalized magnetite (**11**). The magneto-switchable activation of glucose oxidase, GOx, by the functional particles, and using an external magnetic field, is depicted in Scheme 5A. Positioning of the external magnet below the electrode attracts the ferrocene-functionalized magnetic particles to the electrode. Electrochemical oxidation of the ferrocene units generates the ferrocenylium cation that mediates the oxidation of the active site of GOx, thus activating the bioelectrocatalyzed oxidation of glucose. Positioning of the external magnet above the cell retracts the magnetic particles from the electrode. This blocks the electrochemical oxidation of the ferrocene units, and, thus, the bioelectrocatalyzed oxidation of glucose is switched off. Figure 6 shows the cyclic voltammograms of the system consisting of the ferrocene-modified magnetite particles, glucose, and glucose oxidase (GOx), upon positioning the external magnet below (curve a) and above (curve b) the electrochemical cell. Attraction of the magnetic particles to the electrode results in an electrocatalytic anodic current implying that the bioelectrocatalyzed oxidation of glucose is activated. Retraction of the functionalized particles from the electrode by positioning the magnet above the cell, blocks the bioelectrocatalytic function of GOx, and no electrocatalytic current is detected. By the cyclic attraction of the magnetic particles to the electrode, and their retraction from the electrode by means of the external magnet, the bioelectrocatalytic functions of the enzymes are reversibly switched between "ON" and "OFF" states, respectively.

The method to design a system for the magneto-switchable generation of light is schematically presented in Scheme 5B and involves the magneto-switchable generation of chemoluminescence [16]. The aminoethylaminopropylsiloxane-functionalized magnetic particles were reacted with

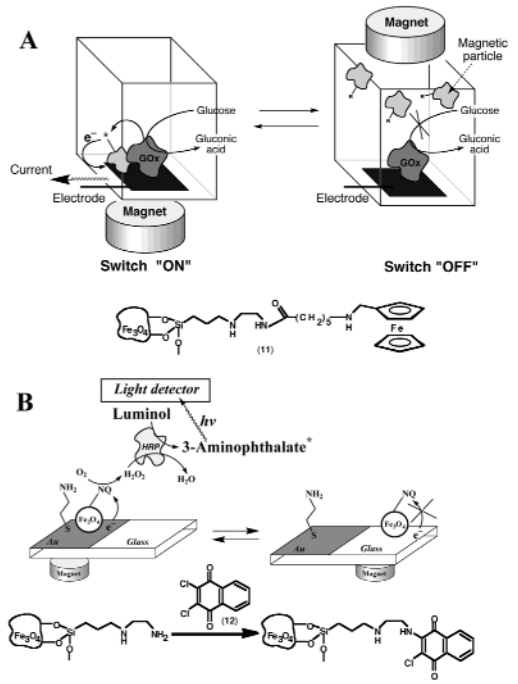


**Scheme 5** Magneto-switchable bioelectrocatalytic and electrocatalytic transformations: (A) magneto-switchable bioelectrocatalyzed oxidation of glucose; (B) magneto-switched electrocatalyzed reduction of $O_2$ and stimulated chemoluminescence.

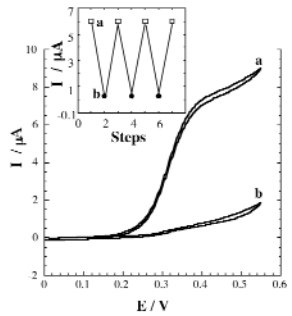


**Fig. 6** Cyclic voltammograms corresponding to the magneto-switched bioelectrocatalyzed oxidation of glucose in the presence of ferrocene-functionalized magnetite particles, 10 mg, and GOx, 1 mg·mL$^{-1}$: (a) magnet below the electrode; (b) magnet above the electrode. Data recorded under Ar, 0.1 M phosphate buffer pH = 7.2, scan rate 5 mV·s$^{-1}$. Inset: Cyclic magneto-switched activation and deactivation of the bioelectrocatalyzed oxidation of glucose by positioning an external magnet below and above the electrode, respectively.

2,3-dichloronaphthoquinone (**12**), to yield the naphthoquinone-modified magnetite particles. Attraction of the quinone-modified particles to the Au electrode results in the reduction of the quinone units and the subsequent catalyzed reduction of $O_2$ to $H_2O_2$. The electrogenerated $H_2O_2$ stimulates the chemoluminescence in the presence of luminol and horseradish peroxidase (HRP). Thus, the light emission is observed when the quinone-functionalized magnetite particles are electrochemically reduced. Translocation of the magnetic particles to the nonconductive glass surface domain, by means of the external magnet, prohibits the electrochemical reduction of the quinone units, and, thus, the electrostimulated chemoluminescence is blocked. Figure 7 shows the magneto-switchable light emission from

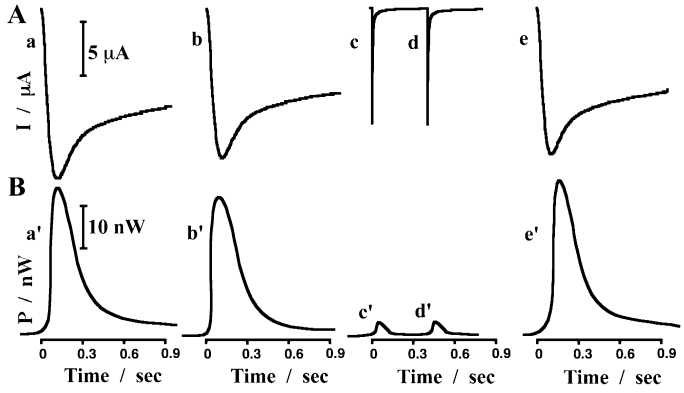


**Fig. 7** Magneto-switchable electrogenerated chemoluminescence using the naphthoquinone-functionalized magnetite particles (10 mg), luminol, $1 \times 10^{-6}$ M, and HRP, 1 mg·mL$^{-1}$; (A) chronoamperometric transients corresponding to the application of potential steps from 0.0 to –0.4 V (vs. SCE) on a cystamine-monolayer-modified electrode where for a, b, and e, the external magnet is positioned below the electrode and for c and d, the external magnet is located above the electrode surface; (B) light emission from the system upon the application of the potential steps described in (A). Curves a′ to e′ correspond to the emitted light signals upon the application of the potential steps shown in curves a to e, respectively. Data were recorded in 0.1 M phosphate buffer, pH = 7.0, under air.

the system using the quinone-functionalized magnetic particles, luminol and HRP, in the presence of an external magnet. Potential steps from 0.0 to –0.4 V are applied on the working electrode. When the functional magnetic particles are attracted to the electrode surface by means of the external magnets, current transients corresponding to the reduction of the quinone units, are observed, Fig. 7A, curves a, b, and e. Concomitantly, light is emitted from the system, Fig. 7(B), curves a′, b′, and e′. Translocation of the functional magnetic particles to the nonconductive surface results in, upon the application of the potential step on the electrode, a minute current transient that originates from the double-layer charging, and from the reduction of residual traces of the quinone-modified magnetic particles on the electrode, Fig. 7B, curves c and d. The translocation of the functional particles to the nonconductive surface blocks the light emission from the system upon the application of the potential steps on the electrode support, curves c′ and d′, respectively. Thus, to stimulate the light emission from the system, the electrocatalytic reduction of $O_2$ by means of the quinone-modified magnetic particles is essential. The magnetic control of electrogenerated chemoluminescence may be used, for example, for the optical imaging magnetic discs.

## CONCLUSIONS AND PERSPECTIVES

The account has described recent advances in the engineering of surfaces with functional metallic, semiconductive, and magnetic nanoparticle architectures. The conjugation of molecular units to the nanoparticles, or the surface assembly of nanoparticles by means of molecular cross-linkers, yield hybrid systems of new chemical or physical functionalities that are missing in the individual components. This was demonstrated by:

- The generation of Au nanoparticle arrays cross-linked by molecular receptors that selectively bind and concentrate an analyte in the receptor cavities. The three-dimensional conductivity of the system enables the electrochemical sensing of the attracted substrate.
- The conjugation of a single Au nanoparticle to a nanoengineered redox enzyme led to its electrical contacting with electrodes, and to the bioelectrocatalytic activation of the enzyme.

- Nucleic acid-functionalized CdS nanoparticles act as a label for the optical imaging and the photoelectrochemical transduction of DNA hybridization.
- Functional magnetite particles were employed for the magneto-switchable activation and deactivation of bioelectrocatalytic processes, and for the magnetically controlled light emission.

In the different hybrid systems, the unique electronic, optical, and magnetic properties of the nanoparticles were coupled to molecular functions of recognition, catalysis, and biocatalysis. These nanostructures led to functional sensing elements and biocatalysts.

## ACKNOWLEDGMENTS

This research is supported in part by the U.S.–Israel Binational Science Foundation (BSF) and the Deutsche-Israelische Program (DIP).

## REFERENCES

1. A. C. Tempelton, W. P. Wuelfing, R. W. Murray. *Acc. Chem. Res.* **33**, 27–36 (2000).
2. A. N. Shipway and I. Willner. *Chem. Commun.* 2035–2045 (2001).
3. C. A. Mirkin, R. L. Letsinger, R. C. Mucic, J. J. Storhoff. *Nature* **382**, 607–609 (1996).
4. S. Chen, R. W. Murray, S. W. Feldberg. *J. Phys. Chem. B* **102**, 9898–9907 (1998).
5. A. N. Shipway, E. Katz, I. Willner. *ChemPhysChem* **1**, 18–52 (2000).
6. M. Lahav, A. N. Shipway, I. Willner. *J. Chem. Soc., Perkin Trans. 2* 1925–1932 (1999).
7. I. Willner, V. Heleg-Shabtai, R. Blonder, E. Katz, G. Tao, A. F. Bückmann, A. Heller. *J. Am. Chem. Soc.* **118**, 10321–10322 (1996).
8. Y. Xiao, F. Patolsky, E. Katz, I. Willner. Submitted for publication.
9. C. M. Niemeyer. *Angew. Chem. Int. Ed.* **40**, 4128–4158 (2001).
10. (a) E. Braun, Y. Eichen, U. Sivan, G. Ben-Yoseph. *Nature* **391**, 775–778 (1998); (b) J. Richter, R. Seidel, R. Kirsch, M. Mertig, W. Pompe, J. Plaschke, H. K. Schackert. *Adv. Mater.* **12**, 507–510 (2000).
11. I. Willner, F. Patolsky, J. Wasserman. *Angew. Chem., Int. Ed.* **40**, 1861–1864 (2001).
12. F. Patolsky, I. Weiss, I. Willner. Unpublished results.
13. F. Patolsky, Y. Weizmann, O. Lioubashevski, I. Willner. *Angew. Chem., Int. Ed.* **41**, 2323–2327 (2002).
14. Z. Wang, K. Shah, T. M. Rana. *Biochemistry* **40**, 6458–6464 (2001).
15. R. Hirsch, E. Katz, I. Willner. *J. Am. Chem. Soc.* **122**, 12053–12054 (2000).
16. L. Sheeney-Haj-Ichia, E. Katz, J. Wasserman, I. Willner. *Chem. Commun.* 158–159 (2002).